Emission-line profiles of helium autoionization states after excitation by fast Li and He ions

P. W. Arcuni*
Physics Division, Argonne National Laboratory, Argonne, Illinois 60439

D. Schneider
Hahn-Meitner-Institute, Glienicker Strasse 100, 1 Berlin 39, Federal Republic of Germany
(Received 9 April 1987)

We report the angle-dependent electron emission from the $(2s^2)^1S$, $(2s2p)^1P$, and $(2p^2)^1D$ autoionizing states of helium, after excitation by 100-keV/amu Li^+, Li^{2+}, and 500-keV/amu He^+, He^{2+}, Li^+, Li^{2+}, and Li^{3+} ions. All of the peak profiles are strongly affected by the electron-ion interaction that occurs after ionization. A method that accounts for this post-collision interaction, and allows comparison with theoretical calculations, is presented, and some previously unexplained discrepancies between theoretical and experimental line profiles are resolved. The differently charged ions cause systematic changes in the observed line profiles. We report some projectile-charge-dependent emission intensities for the different peaks. Accurate energy differences between the excited states are reported.

I. INTRODUCTION

We have experimentally studied the electron emission peaks of three autoionization states of He—$(2s^2)^1S$, $(2p^2)^1D$, and $(2s2p)^1P$—after excitation by singly, doubly, and triply charged ions with MeV energy. In this paper we are primarily concerned with the emission-angle-dependent profiles and line intensities. It is experimentally apparent that the interaction between the emitted electron and the fast ion (which is moving faster than the electron) significantly affects the peak profile.[1] We demonstrate that inclusion of this effect enhances agreement between experiment and theory for these emission profiles. We also have studied the profiles and emission amplitudes of these states as a function of the total charges of, and number of electrons carried by, several equal-velocity ions. The data presented here should help to provide a good test of the theoretical understanding of the excitation process.

It has long been known that autoionization states generally have absorption and emission lines that are asymmetric in observed energy. These line profiles are a consequence of the quantum interference between the discrete autoionization state and the continuum in which it is embedded.[2] This behavior is generally well understood; comparison of theory with the experimental profile sensitively tests the system being studied.[2] In the particular case of electron emission lines from atoms that have been excited by fast ions, the profile calculation is particularly difficult.[3–6] The transition matrix elements between the ground state and the autoionization state, between the ground state and the continuum, and between the autoionization state and the continuum are necessary. This requires an extensive understanding of the excitation and ionization process. Because this understanding is usually not present, a standard simplification has been to assume that the excitation process is quick and small. This leads, in general, to the use of the first Born approximation.

Several profile calculations using the first Born approximation have been made for excitation by electrons and protons. Of particular interest to us are the calculated profiles of the $(2s^2)^1S$ and $(2s2p)^1P$ states of helium after excitation by 100-keV and 500-keV protons.[5,6] To our knowledge there are no calculations that involve excitation by heavier ions.

One purpose of the experiment reported here is to test the above calculations. We also wanted to use projectiles that have velocities and charges such that the use of the first Born approximation becomes questionable. Of course, such a study would challenge the theoretical profile calculations. What effect any electronic structure of the projectile may have on the excitation process, and thus on the profiles, is also of interest. To this purpose we used several projectile ions: 100-keV/amu Li^+ and Li^{2+}, and 500-keV/amu He^+, He^{2+}, Li^+, Li^{2+}, and Li^{3+}. The target in all cases was helium. Also available to us were some previously unpublished experimental results of the excitation of the same states by 500-keV H^+ and 100-keV/amu H^+, He^+, and He^{2+}.[7,8] We present the observed line profiles at several angles between 18° and 155° with respect to the projectile ion beam.

These are the first reported experimentally determined profiles, and intensities, of these states using any lithium ion projectile, and the first using helium ions at these collision velocities. There have been some experimental results using protons[7–14] and some using helium atoms and ions at smaller velocities.[8,15,16] Our electron energy resolution is 0.115 eV [full width at half maximum (FWHM)], which is better than most of these previous studies.

We also present the observed projectile charge dependence of the spectral line intensities. To first order in perturbation theory, the excitation of doubly excited

states is a correlation effect. One would then expect the excitation to vary as the square of the projectile charge Q, as is often the case for optically allowed single-electron excitation. In higher-order perturbation theory the correlation is not necessary, and excitation can show a different dependence on projectile charge. In the case of second Born dominated excitation the intensity should vary as Q^4. The charge dependence of the excitation is then a naive measure of the amount of correlation present in the excitation, a subject of great interest in atomic physics. We have found dependences that vary sharply from state to state and depend sensitively on ion charge and velocity. These data are difficult to interpret, however, because of obvious interference effects.

Also reported are highly accurate energy differences between the $(2p^2)^3P$ and $(2p^2)^1D$ states and also between the $(2s^2)^1S$ and $(2p^2)^1D$ states. These values are compared with theory and previous measurements.

Finally, the profile analysis used here is unique and requires some explanation. The uniqueness is mandated by a post-collision interaction at fast-ion velocities only recently considered.[1] The line profiles are affected by the fast-ion post-collision interaction (FIPCI) for all the projectiles studied. The extremely strong peak distortions caused by some projectiles (e.g., 700-keV Li^{2+}) are discussed.

II. THE EXPERIMENT

The experimental apparatus is very similar to that presented previously.[1] A singly charged ion beam of between 0.2 and 2.0 mA was produced by the Argonne National Laboratory 4.5-MV Dynamatron Accelerator. The beam passed through 6° and 20° bending magnets before reaching the target. Several collimators along the beam line reduced the angular divergence of the beam to between 0.3° and 0.6° and the cross section of the beam to about 2.0×2.0 mm. If necessary the beam ions could be passed through a thin foil or through a gas cell in order to obtain more highly charged ions. This stripping was done between the two bending magnets which momentum analyzed the ions. The ions were thus well-characterized in the collision region. Outside of the stripping cell and target chamber the pressure was about 3×10^{-7} Torr.

The helium target was maintained by a gas jet consisting of a small brass tube, perpendicular to the ion beam, with an inner diameter of 1.2 mm which was located about 3.0 mm above the beam center. The helium gas flow was controlled by a precise and very reliable leak valve. The pressure inside the target chamber, without the gas jet, was about 3×10^{-7} Torr. When the gas jet was on, the ambient pressure was maintained at 2×10^{-4} Torr. By comparing the signal count rate when the gas jet was on to when the chamber was flooded by a uniform, ambient helium gas pressure of 2×10^{-4} Torr, it was determined that the target density in the jet was about ten times the ambient density.

Two parallel-plate electrostatic spectrometers[17,18] could be rotated about the intersection of the ion beam and the gas jet. The electron energy was measured by scanning the voltage between the plates. Doubly differential cross sections, in both angle and energy, could therefore be measured. After being energy analyzed the electrons were directed into an 18-dynode electron multiplier for amplification. The signal was further amplified, digitally counted, and recorded in a multichannel scaling mode by an on line PDP-11/45 computer. A Faraday cup collected the ion beam, and the total charge was integrated to normalize the beam exposure for each data point. All objects inside the chamber were made of nonmagnetic materials and the chamber was surrounded by μ metal. Metal surfaces close to the target and inside the spectrometers were coated with conductive graphite.

Experimentally measured, proton-induced ionization of helium was compared to previously published doubly differential ionization cross sections.[19] The resulting normalization constants were used to determine the ionization cross sections caused by the other ions. The cross-section values reported here have an estimated error of $\pm35\%$.

Figure 1 shows a survey spectrum of the doubly excited system. In this figure there is a large amount of triplet excitation. For faster projectile ions, or those with more tightly bound electrons, the $(2s2p)^3P$ peak is rarely present. The $(2p^2)^1D$ and $(2s2p)^1P$ peaks are usually dominant, with the $(2s^2)^1S$ peak present at a lesser intensity.

As can be seen in Fig. 1, the $(2p^2)^1D$ and $(2s2p)^1P$ peaks, called hereafter the ^1D and ^1P peaks, lie close together and overlap. They are in fact separated by about 237 meV and have natural widths of about 37 and 63 meV, respectively.[20] As might be expected, we found that the profile determination of these two peaks was

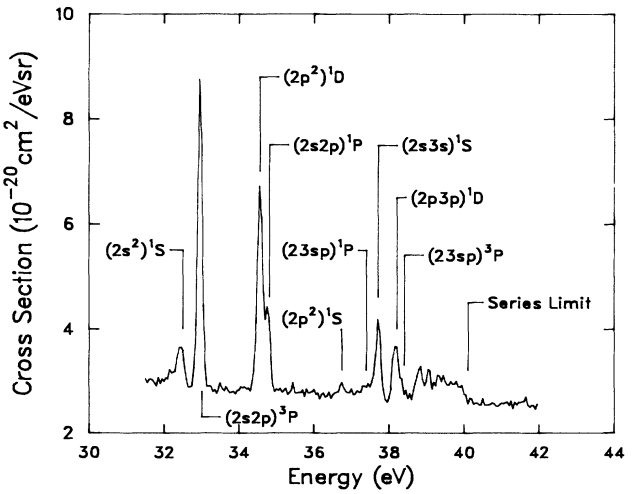

FIG. 1. A survey spectrum of the $(2lnl')^{1,3}L$ doubly excited helium states. This spectrum was taken at an angle of 155° with respect to the 700-keV $^7Li^+$ beam used to excite the helium target. This paper experimentally studies the intensities and profiles of the $(2p^2)^1D$, $(2s2p)^1P$, and $(2s^2)^1S$ states for the different ions used to excite them.

very sensitive to the energy resolution of the electron spectrometers.

We used the least-squares technique[21,22] to determine the percent errors of, and the correlations between, the parameters as functions of the spectrometer resolution. Using simulated spectra of the same total acquisition time, it was found that the percent errors of the parameters rapidly increase for spectrometer resolutions worse than about 0.12 eV (FWHM). Correlation coefficients effectively equal one for similar resolutions.[23]

In our case the resolution of the spectrometers was 0.115 ± 0.006 eV. This value was confirmed through analytic theory, computer models, and experimental tests.[23]

III. THE PARAMETRIZATION EQUATION

A. The parametrization

While the emission profiles we observed are distorted by a post-collision interaction (PCI), we first present parametric equations of undistorted profiles. We do this because such parametrizations will be essential to an understanding of the derived parameters that will be presented later.

One of the most common and useful parametrization that describes undistorted peaks is called the Shore parametrization[24,25] (unless otherwise noted, all units will be atomic units throughout this paper),

$$\frac{d^2\sigma}{d\theta dE}=F(E,\theta)+\sum_r \frac{A_r(\theta)\varepsilon_r+B_r(\theta)}{1+\varepsilon_r^2} , \tag{3.1}$$

where

$$\varepsilon_r=2(E-E_r)/\Gamma_r . \tag{3.2}$$

E is the observed electron energy and E_r is the resonance position of the state being observed. Γ_r is the natural width (FWHM) of that state. θ is the emission angle relative to the ion beam. The Shore parameters are $A_r(\theta)$ (called the antisymmetric Shore parameter) and $B_r(\theta)$ (called the symmetric Shore parameter). Of course, these parameters are different for different projectiles. The background function $F(E,\theta)$ is usually fit with a linear or quadratic function of the energy. The fit of the background has little effect on the other parameters if the background is measured far from the peak. The Shore parametrization is usually preferred for fitting purposes because A_r and B_r are linear.

The antisymmetric and symmetric Shore parameters can be represented in theory as functions of the transition matrix elements between the ground state and the autoionization state, between the ground state and the appropriate partial wave of the continuum, and between the various partial waves of the continuum.[3] This is in direct contrast to the scattered particle observation channel (such as in photoabsorption), where, because of the necessary integration over the emitted electron momentum, only the partial wave with the same angular momentum quantum number as the discrete peak is involved in the interference.[2,3]

An alternative representation for the peak profiles is the Fano parametrization, so called because of its seminal use in the analysis of autoionization profiles of states that were studied through photoabsorption and electron-loss measurements.[2,26] It is written

$$\frac{d^2\sigma}{d\theta dE}=F_F(E,\theta)+\sum_r \frac{\tilde{\sigma}_r(\theta)[\tilde{q}_r(\theta)+\varepsilon_r]^2}{1+\varepsilon_r^2} , \tag{3.3}$$

where $F_F(E,\theta)$ is the incoherent background while $\tilde{\sigma}_r$ is the coherent background parameter. $\tilde{q}_r$ is a dimensionless parameter that conveniently measures the shape of the profile but is independent of the magnitude of the cross section. When the absolute value of $\tilde{q}_r$ is large, the peak is Lorentzian, and when it is equal to zero, the peak is a symmetric window, or dip. For intermediate values of $\tilde{q}_r$ the profile is asymmetric. Note that because of the different observation channel $\tilde{q}_r$ is not the same as what is sometimes called the Fano q value.

The Fano parametrization and the Shore parametrization are equivalent.[2,3] There is a simple transformation of one set of parameters to the other. Despite this equivalence, however, they each have their own advantages. In particular, $\tilde{q}$ of the Fano set is very helpful when looking at qualitative trends in profile behavior, and as a marker of significant spectral features: a window of a particular peak is unambiguously identified whenever $\tilde{q}=0$. The presence of a window in the Shore parametrization is not so immediately evident. As discussed, $\tilde{q}$ is independent of cross section, and we have no need to worry about normalization factors when comparing our data to independent experiments. On the other hand, when Eq. (3.1) is integrated over energy, one finds that the result is proportional to the Shore parameter B. B is thus of use when comparing emission yields when different fast ions are used.

In this paper we are concerned with two different aspects of the measured peaks: their shape and their size. These aspects are best measured by $\tilde{q}$ and B, respectively, and we will casually mix the discussion of both parameters, even though they come from different parameter sets.

It was pointed out earlier (Ref. 1) that the profiles can be distorted by projectile ions that are relatively fast (i.e., energies of several hundred keV/amu). In fact, we have found that all of our spectra are affected by what we call a fast-ion post-collision interaction, or FIPCI. This occurs when the excited atom decays while the field of the outgoing ion is still significant. Since the emitted electron is moving more slowly than the projectile ion, it will be accelerated if emitted toward the ion, and decelerated if emitted away from the ion. Thus, the effect of the ion on the electron will depend on the angle of observation. The FIPCI is qualitatively different from the standard Barker-Berry model of PCI,[27] where the velocity of the ion is much less than that of the emitted electron. In that case the change in electron energy is independent of the emission angle.

In the development of the FIPCI we will consider an autoionization electron that would have a final velocity $\mathbf{v}_0$ without any PCI. At the time of autoionization t', however, it is subject to the electric field of a fast, heavy

ion of charge Q and velocity $\mathbf{V}$. It is assumed that the fast ion is not affected by any PCI, and that the effect of the remnant He^+ ion on the electron is included by the above assumption about $\mathbf{v}_0$. Clearly the final energy of the electron will be affected by the time of its emission, the velocity of the ion (as reflected by the distance between the electron and the ion), and by the time of interaction, which depends on the relative electron-ion velocity. In this classical picture we can develop an accurate approximation of the change in energy of the emitted electron in the laboratory frame of reference,[28–30]

$$\Delta E \approx \frac{-Q}{V(t'-t_0)}\left[1-\frac{V}{|\mathbf{V}-\mathbf{v}_0|}\right]=\frac{C}{V(t'-t_0)} . \quad (3.4)$$

t_0 is the time of excitation of the autoionizing state (and presumably the time of closest approach of the ion to the atom). Equation (3.4) is not the same as the analogous equation for ΔE that was presented in an earlier paper.[1] That paper made the unnecessary assumption that the transverse velocity of the electron (relative to the electron-ion axis) was unchanged by the FIPCI. Equation (3.4) is superior in that it applies to the velocity regime $V<v_0$. It is also more accurate in the velocity regime $V>v_0$ considered in this paper.

In what follows the strength of the electron-ion interaction is measured by the magnitude of C/V, which is of course not a parameter since its components are known. The parametrization equation that follows is written in terms of C/V, and as long as Eq. (3.4) can be written as a constant over time, the form of that parametrization is independent of the particular formula that determines the value of that constant.

Of course, the observed peak is the result of electrons emitted at all times. The emitted electrons will also interfere with the continuum electrons produced by direct ionization. These effects are included in the profile equation presented earlier.[1,31] The parametric equation from Ref. 1 is thus (with angular dependence suppressed)

$$\frac{d\sigma}{d\theta\, dE}=F_F(E)+|a|^2+\sum_r\left\{\frac{2}{\Gamma_r}\frac{|b_r|}{1+\varepsilon_r^2}\frac{C}{V\sinh\left[\frac{\pi C}{V}\right]}\exp\left[\frac{\pi C}{V}-\frac{2C}{V}\tan^{-1}\left[\frac{1}{\varepsilon_r}\right]\right]\right.$$
$$+\left[\frac{\Gamma_r}{2\pi}\right]^{1/2}\frac{8|a||b_r|}{\Gamma_r^2(\varepsilon_r^2+1)}\left|\Gamma\left[1+\frac{iC}{V}\right]\right|\exp\left[\frac{\pi C}{2V}-\frac{C}{V}\tan^{-1}\left[\frac{1}{\varepsilon_r}\right]\right]$$
$$\left.\times\left[\sin(\alpha_r)\frac{\Gamma_r\varepsilon_r}{2}+\cos(\alpha_r)\frac{\Gamma_r}{2}\right]\right\}, \quad (3.5)$$

where

$$\alpha_r=\frac{-C}{2V}\ln\left[(\varepsilon_r^2+1)\frac{\Gamma_r^2}{4}\right]+\arg\left[\Gamma\left[1+\frac{iC}{V}\right]\right]+E\delta_r , \quad (3.6)$$

$$F_F(E)=F_0+F_1E+F_2E^2 ,$$

and

$$0\le E\delta_r\le 2\pi ,$$
$$E_0(^1P)=E_0(^1D)+0.237\ \text{eV} , \quad (3.7)$$
$$F_F(E)\ge 0 .$$

$\Gamma(1+iC/V)$ is a Γ function. We call $|b_r|$ the emission amplitude parameter and δ_r the phase parameter. $|a|$ is the coherent background parameter, assumed the same for all peaks in the spectrum. E_r is the resonance energy parameter and F_0,F_1,F_2 are the linear parameters used to fit the background. All other quantities in Eqs. (3.5)–(3.7) are fixed to known values.

We fixed the energy difference between the ^1D and ^1P peaks to the known value of 237 meV.[20] This improved the fit convergence and did not affect the fit quality. Finally, we limited the phase parameter δ_r and the incoherent background $F_F(E)$ as in Eq. (3.7). Equation (3.5) was numerically integrated with a spectrometer transmission function of known width and shape. The calculated parameters showed little sensitivity to changes in the integration step size or to small changes in the transmission function itself.

B. The derived parameters

The FIPCI was not included in previous theoretical calculations of the emission profile parameters of the doubly excited states of helium.[5,6] The form of the parametric equation, Eq. (3.5), was thus not anticipated. Comparison of our results with theory is therefore difficult. If theoretical profile predictions that include the FIPCI are unavailable, a next best solution may be for the experimentalist to know what the profile would be if there were no FIPCI. We tentatively present a way to do this using the fitted parameters of Eq. (3.5). Evidence presented in later sections will give justification for this procedure.

In the limit when the distortion factor goes to zero, that is, when $C/V\to 0$, Eq. (3.5) becomes

$$\frac{d\sigma}{d\theta\, dE}=F(E)+\sum_r\left[\frac{(2/\Gamma_r\pi)\,|b_r|^2+(\Gamma_r/2\pi)^{1/2}(4/\Gamma_r)\,|a|\,|b_r|\cos(E\delta_r)}{\varepsilon_r^2+1}+\frac{(\Gamma_r/2\pi)^{1/2}(4/\Gamma_r)\,|a|\,|b_r|\sin(E\delta_r)\varepsilon_r}{\varepsilon_r^2+1}\right]. \tag{3.8}$$

Equation (3.8) is equivalent to the Shore parametrization, Eq. (3.1), with

$$A_r'(\theta)=2(2/\Gamma_r\pi)^{1/2}\,|a|\,|b_r|\sin(E\delta_r)\,,$$
$$B_r'(\theta)=\frac{2\,|b_r|^2}{\Gamma_r\pi}+2\left[\frac{2}{\Gamma_r\pi}\right]^{1/2}|a|\,|b_r|\cos(E\delta_r)\,. \tag{3.9}$$

The above "Shore parameters" are labeled with primes to indicate that they are derived from Eq. (3.5) in the limit when $C/V\rightarrow 0$; they are not measures of the actual peak profile. These primed parameters are called limit parameters for convenience. We use the limit Shore parameters to calculate the limit Fano parameters, $\tilde{q}\,'$ and $\tilde{\sigma}\,'$.

Equation (3.5) is not an ideal parametric equation. In particular, there is a large correlation between the coherent background parameter $|a|$, the peak amplitude parameter $|b_r|$, and the phase parameter δ_r. Large variations of the various parameters are thus allowed and error estimates of the original parameters are difficult. Nevertheless, the limit parameters discussed here seem to describe concrete observable aspects of the peak profiles. As such, they are particular combinations, of the original parameters, that do not seem to be (very) affected by the correlations of the original parameters. Not only are they valuable for comparisons to previous experiments and to theory, but they are convenient for comparisons of different spectra with each other. Error propagation is nonetheless difficult, and internal consistency of the data is the only guide to the errors of the data presented here.

IV. THE EFFECT OF FIPCI ON THE OBSERVED PROFILES

A. Small values of C/V ($0\leq C/V\leq 0.1$)

In Fig. 2(a) we show the emission profile observed at 30° after the helium target was excited by 2-MeV He^+. It was demonstrated earlier[1] that this profile was apparently well-fit by the Shore formula [Eq. (3.1)]. Nevertheless, in this figure we show the fit from Eq. (3.5) and the limit profile derived from it. Note that the limit profile of the combined peak (both the ^1P and ^1D states) has the opposite asymmetry of that shown by the true profile. In Fig. 2(b) we show the emission profile at 90°. Again the projectile is 2-MeV He^+. This fit also uses Eq. (3.5). In this case, however, C/V is small, and the limit profile and the true profile are similar. Note that the true profile at 90° has the same direction of asymmetry as the limit profile of the 30° spectra.

When other projectiles of the same velocity are used, this behavior of the ^1D-^1P peak is repeated, that is, the peaks have a dip to the high-energy side when observed at 90°, but a dip to the low-energy side when observed at some smaller angles. The limit profiles, however, always have a dip to the high-energy side for all forward angles. The angle when the actual dip changes side, that is, when the peak appears symmetric, occurs at an angle such that $0.02<C/V<0.07$. Thus when the projectile charge is increased the symmetric peak occurs at larger angles [see Eq. (3.4)].

Plotted in Fig. 3(a) are the $\tilde{q}$ values of the ^1P peak that were obtained from a direct fit of the spectra using the non-FIPCI equation, Eq. (3.1), both for excitation by 2000-keV $^4He^+$ (observed in this study) and after excitation by 500-keV H^+ (observed by Ridder[7]). These two

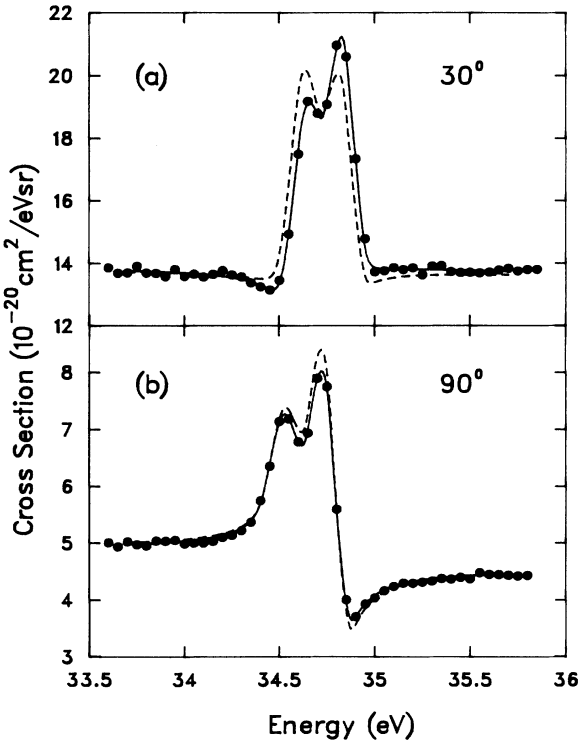

FIG. 2. Electron emission of the $(2s^2)^1P$ and $(2p^2)^1D$ peaks after 2.0-MeV $^4He^+$ excitation. The spectra observed at 30° with respect to the ion beam (a) and at 90° with respect to the ion beam (b). In each case the solid line is a fit of the data using the FIPCI equation (3.5). The dashed line is the mathematical limit of that fit when the magnitude of the ion-electron post-collision interaction is taken to zero.

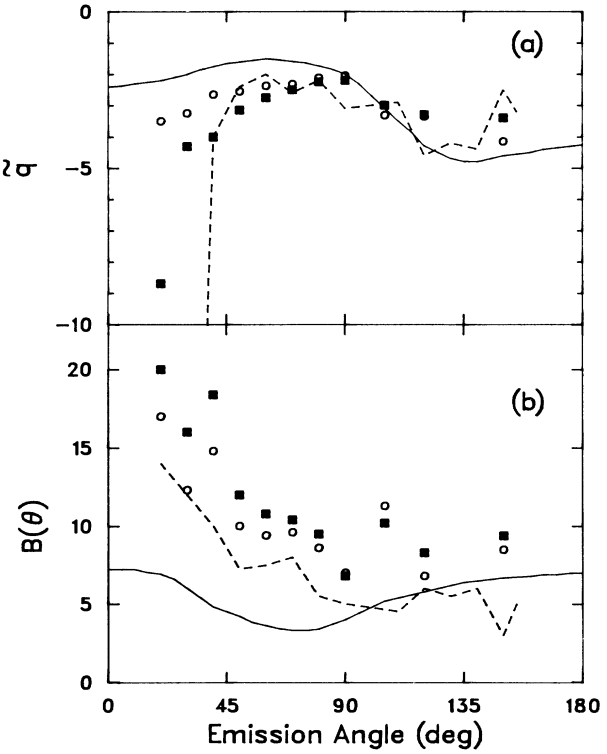

FIG. 3. Fitted and derived parameters of the $(2s2p)^1P$ peak of helium after excitation by some singly charged ions of 500 keV/amu. (a) The Fano shape parameter $\tilde{q}$. (b) The symmetric Shore parameter $B(\theta)$ in units of 10^{-20} cm^2/eV sr. The squares are a direct application of Eq. (3.1) on 2000-keV He^+ ion data, the dashed lines were similarly obtained by Ridder (Ref. 7) for 500-keV H^+ ion data, the open circles result from a fit of the 2000-keV He^+ data [by Eq. (3.5)] that was subsequently taken to the limit where the FIPCI goes to zero (see text), and the solid lines are theoretical predictions for excitation by 500-keV H^+ (Ref. 5).

curves behave similarly, in particular, at forward angles $\tilde{q}$ diverges, that is, the ^1P peak becomes symmetric. Also shown are the $\tilde{q}'$ values obtained from the He^+ excitation measurements. Note that the divergence of this paper at forward angles is greatly reduced. Finally, the theoretical calculations of this parameter for 500-keV H^+ excitation[5] is shown. The limit parameters match the theoretical calculations much better than the real profiles do.

The above information hints that the low-energy dip observed at forward angles is induced by the FIPCI and that the limit parameters may be used to compare experimental results with current theoretical calculations. This conclusion is supported by observations in the next section.

In Fig. 3(b) the parameter shown is the symmetric Shore parameter, $B(\theta)$. In this case use of the limit procedure does not greatly improve the agreement with theory. Why this is so is not obvious, but it seems clear that at least for this kinematic situation, and for this peak, the FIPCI predominantly affects the symmetry of the peak but not its gross size. The various experimental measurements of the symmetric Shore parameter all agree on a large increase toward forward angles.[7] Therefore, we consider it likely that the forward angle increase that is shown in Fig. 3(b) is not caused by FIPCI nor by experimental error, and is instead intrinsic to the excitation process. If this is true then the theoretical calculations are in some error.

B. Moderate distortion factors ($C/V \sim 0.9$)

Figure 4 shows the same parameters as Fig. 3 for a projectile velocity of 100 keV/amu. The values of C/V are correspondingly larger. In Fig. 4(a) the apparent profile of the ^1P peak becomes symmetric at about 45°. The ^1P peak has a dip to the right for observation angles greater than that angle, and a dip to the left for angles less than that. This is entirely analogous to the behavior with the faster projectiles discussed above. In this case the limit profiles entirely eliminate the divergence of $\tilde{q}$—a divergence that is not predicted by theory. Note the interesting result that $\tilde{q}$ is zero at about 25°, corre-

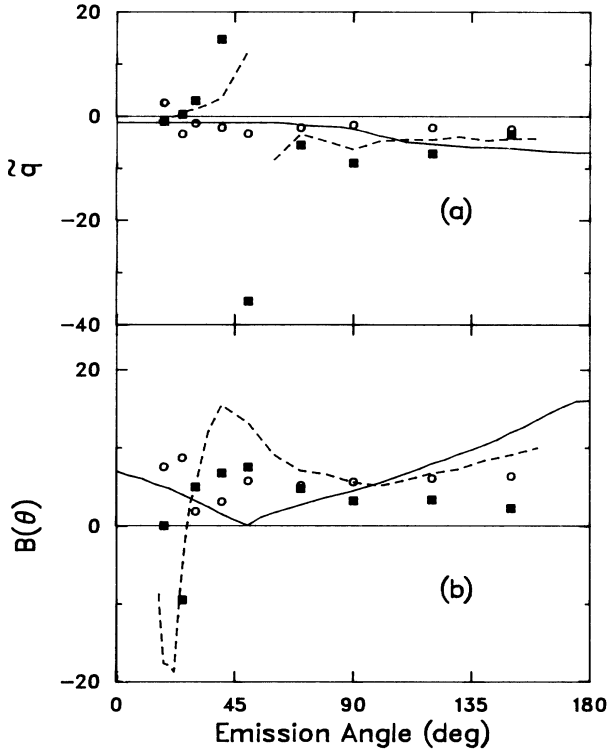

FIG. 4. Fitted and derived parameters of the $(2s2p)^1P$ peak of helium after excitation by some singly charged ions of 100-keV/amu energy. The points and lines have the same significance as in Fig. 4, except that the data points refer to excitation by 700-keV Li^+ ions, and the lines refer to excitation by 100-keV H^+. The solid curve was obtained from Ref. 5, the dashed-curve data from Ref. 8.

sponding to a symmetric window resonance. This is a result of the low-energy dip becoming larger and larger, until only the dip remains. Again the limit profiles do not reproduce the window and the window is not predicted by theory.

The window at 25° is indicated by a negative value of the apparent symmetric Shore parameter in Fig. 4(b). Again the limit parameters do not show a window and improve agreement with theory.

Bordenave-Montesquieu *et al.*[14] have introduced "annulment diagrams" to summarize the profile data that they and Ridder[7] have accumulated for proton excitation. These diagrams show the positions of symmetric peaks as lines in proton-energy and electron-emission-angle space. In their annulment diagram for the ^1P peak, two lines are evident at energies greater than 100 keV. One of these plots the position of symmetric Lorentzian peaks. It "predicts" a symmetric peak at 20° for 500-keV protons. The apparent divergence of $\tilde{q}$ For the 2000-keV $^4He^+$ data clearly belongs on this line. The other line gives the positions of symmetric windows. It predicts a symmetric window at an emission angle of about 20° for 100-keV H^+ proton excitation. The window observed in Fig. 4 belongs on this line.

The symmetric peak observed here at 45° after 700-keV Li^+ excitation, and in the data by Prost for 100-keV H^+ excitation[8] [Fig. 4(a)], is not shown in the annulment diagram. The first curve, however, comes close to the observed position (i.e., 100 keV/amu at $\sim$45°). The discrepancy may be attributable to the ionic structure or to experimental error in the previous work.

The above paragraphs lead to two conclusions: First, the gross apparent features of the ^1P peak profiles are roughly independent of the electronic structure (but not the total charge) of the ion. Even 700-keV Li^+ excitation appears similar to 100-keV H^+ excitation. Second, and related to the above comment, much of the profile dependence in this velocity range is attributable to the FIPCI. In other words, at least two curves in the annulment diagram of Bordenave-Montesquieu *et al.* are caused by the post-collision interaction.

C. Large distortion factors ($C/V \gtrsim 1.7$)

Figure 5 shows the observed, fitted, and limit profiles of the ^1D and ^1P states observed at an emission angle of 20°. The excitation ion was 700-keV Li^{2+}. In this case $C/V=1.7$, which is considerably larger than the values of C/V discussed previously. Unfortunately no theoretical predictions of these profiles are available, but some interesting features are still evident.

First, the apparent peak intensity is somewhat smaller and broader than the limit peak intensity. The reason for this is obvious, since peak electrons that would be concentrated in a narrow energy range, without FIPCI, become spread over a broader energy range. This effect would of course be more apparent as C/V increases, as happens when the observation angle is decreased (at 0° $C/V=4.0$). This is one reason that peak profiles at forward angles are often more difficult to measure than they are at backward angles. The large background usually present at forward angles further obscures the (smaller) peak.

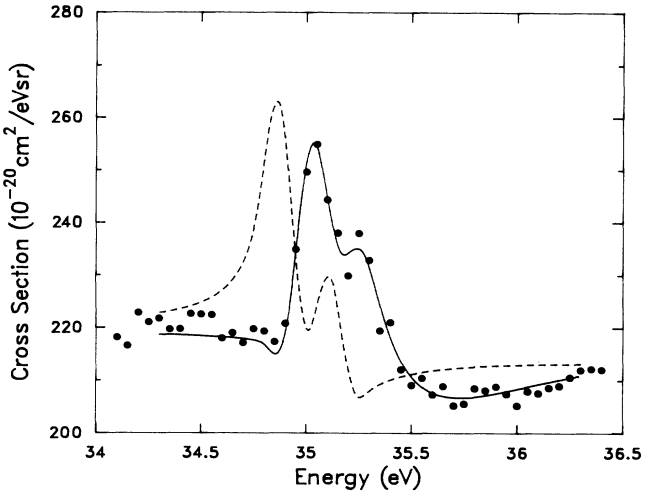

FIG. 5. The emission spectra of the $(2s2p)^1P$ and $(2p^2)^1D$ peaks, observed at 20°, after excitation by 700-keV Li^{2+}. The points are the measured data, the solid line is a direct fit using the FIPCI equation [Eq. (3.5)], and the dashed line is the limit profile (see text).

Second, it is evident that the nominal peak positions are shifted in energy. Since the ^1D and ^1P states have different lifetimes they will be shifted differently, with the shorter-lived ^1D peak being shifted more than the ^1P peak [this lifetime-dependent shift also occurs in the Barker-Berry theory of PCI (Ref. 27)]. Profile measurements at forward angles are again made more difficult, since the net result is a merging of the two peaks.

Finally, since the value of C/V changes rapidly with angle at small observation angles, the emission profiles will change rapidly also. In that case the finite acceptance width of the spectrometer becomes significant. For instance, in Fig. 5 the value of C/V changes by 34% across the $\pm 3°$ acceptance angle of the spectrometer. This could cause a significant experimental problem.

The large discrepancies between the theoretical profile parameters and the experimental profile parameters, especially at forward angles, have not been understood for several years.[6–8,13,14] In addition, previous measurements of profile parameters[7,12,14,15] at similar ion velocities have shown strong variations of the profiles as a function of the observation angle, particularly at small angles. The same and other studies have shown similar variations as a function of projectile velocity. It is now clear that much of this discrepancy can be explained by variation of the FIPCI distortion factor, C/V. This is in apparent contrast to some reports that attribute this behavior to strong variations of the continuum wave functions.[6,32]

D. Possible errors in the FIPCI model

One assumption in the derivation of Eq. (3.7) is that the electron velocity v_0 is independent of the distance

from the residual ion. The velocity of the electron, however, should be larger when it is closer to the residual He^+ ion. Figure 5 shows some distortion at least 1.4 eV from the nominal peak position. For each an energy shift, Eq. (3.4) would place the Li^{2+} ion about 66 a.u. from the helium atom at the time of decay. If, however, v_0 were 1.72 a.u. (the velocity the electron would have at a distance 5 a.u. from the helium ion), Eq. (3.4) gives a change in energy of 1.8 eV. Of course, the velocity of the electron will drop rapidly to its final value as it moves away from the He^+ ion, and the model should integrate over time to include this effect. Simple numerical simulations confirm errors of the magnitude discussed above.

It was demonstrated earlier, for the states studied here and at these projectile velocities, that state-state interference is probably negligible. In some cases, however, particularly when the background is small, Eq. (3.5) should include this interference.[28] In addition, the derivation of Eq. (3.5) should also include an integration over the ion-atom impact parameter, but this should not affect the ability of Eq. (3.5) to fit a peak profile.

Finally, it is important to stress that this method of comparison to current theoretical models is inherently unsatisfactory. A fully quantum-mechanical model that can predict the true line shapes would be preferable.

V. EXPERIMENTAL RESULTS

A. The $\tilde{q}'$ parameter

Figures 6, 7, and 8 compare the limit Fano profile parameters of the three studied peaks after excitation by several 500-keV/amu projectiles. We pointed out above that ions of the same charge create very similar profiles. Secondly, while inclusion of FIPCI reduces the difference, ions of different charge can still produce significantly different effects. For instance, in Fig. 6 it appears that ions of higher charges produce more symmetric ^1P peaks. The triply charged Li^{3+} ion causes the ^1P peak to become considerably more symmetric than the other four projectiles studied. Figure 7 shows that, for the ^1S peak, the higher charges cause the backward angle asymptote of $\tilde{q}'$ to shift to more forward angles. This asymptote, which for the H^+ ion is predicted to occur at about 145° (Ref. 6) (and in an experiment using H^+ ions occurs at 130°)[12] occurs between 120° and 150° for He^+ projectiles, between 90° and 115° for Li^{2+} and He^{2+} projectiles, and between 70° and 90° for Li^{3+} projectiles. A different behavior is observed for the ^1D peak, shown in Fig. 8. In this case, the He^+ and Li^+ data show an asymptote between 80° and 90°. $\tilde{q}'$, which is positive at forward angles, becomes negative at backward angles (the positive value of $\tilde{q}'$ for the Li^+ ion at 150° may be an error caused by the difficulty in fitting the very small peak at that angle). For more highly charged ions, however, the asymptote disappears, and $\tilde{q}'$ remains positive over the entire angular range, though it does get large at about 90°.

In the case of the ^1S peak the asymptote of $\tilde{q}'$ at backward angles (where also $\tilde{\sigma}' \rightarrow 0$) is caused only by

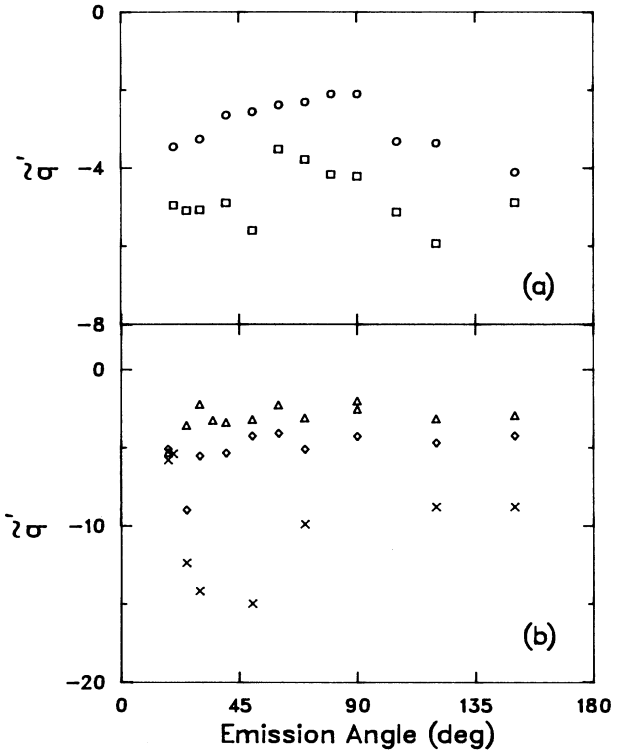

FIG. 6. The limit Fano shape parameter $\tilde{q}'$ as a function of emission angle for the $(2s2p)^1P$ state of helium. (a) ○, 2000-keV $^4He^+$; □, 2000-keV $^4He^{2+}$. (b) △, 3500-keV $^7Li^+$; ◇, 3500-keV $^7Li^{2+}$; × 3500-keV $^7Li^{3+}$.

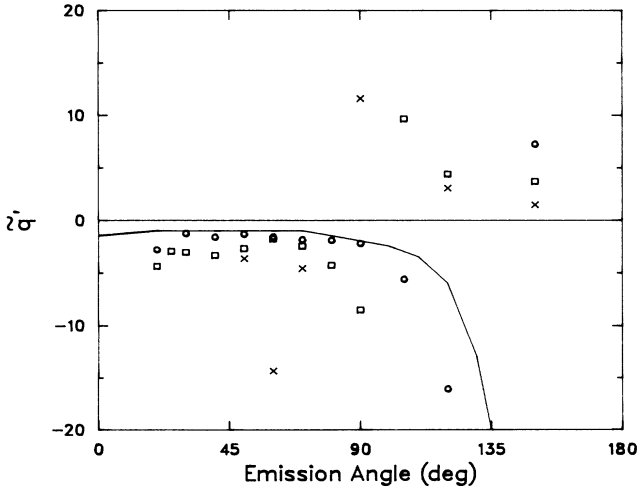

FIG. 7. The limit Fano shape parameter $\tilde{q}'$ of the $(2s^2)^1S$ state. ○, 2000-keV $^4He^+$; □, 2000-keV $^4He^{2+}$; ×, 3500-keV $^7Li^{3+}$. The solid line is the theoretical prediction of $\tilde{q}$ for 500-keV H^+ excitation (Ref. 6).

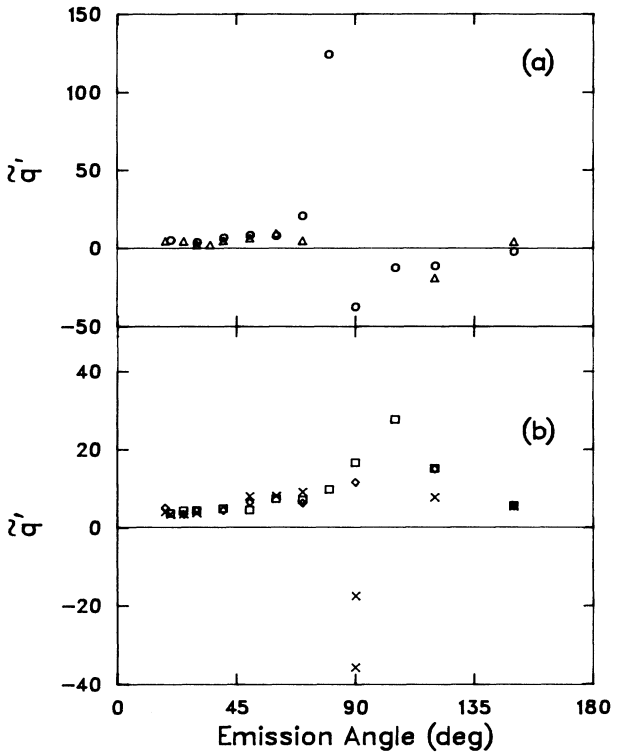

FIG. 8. The limit Fano shape parameter of the $(2p^2)^1D$ state. (a) Excitation by singly charged ions: ○, 2000-keV $^4He^+$; △, 3500-keV $^7Li^+$. (b) Excitation by doubly and triply charged ions: □, 2000-keV $^4He^{2+}$; ◇, 3500-keV $^7Li^{2+}$; ×, 3500-keV $^7Li^{3+}$.

interferences between the autoionized level and the S wave of the continuum, and by interferences between the S wave and the other partial waves.[6] The angular behavior of the peak profile is therefore very sensitive to state-continuum interference. It is evident in Fig. 7 that changes occur as the projectile charge is increased. A possibly analogous behavior is shown in Ref. 6, where the behavior of the profile is studied as a function of the energy of an incident electron. Apparently the interferences are such that the asymptote of $\tilde{q}$ moves to more forward angles as the electron energy is decreased (or as the interaction strength is increased). In Fig. 7 the asymptote moves to more forward angles as the ion charge is increased (and again as the interaction strength is increased). Smaller projectile energies (and larger projectile charges) cause relatively more partial waves to affect the interference.

Presumably the same factors that affect the ^1S profile would also affect the profile of the other states. Since these states decay into different partial waves, and because the excitation mechanisms are different, the manifestations of the interferences may very likely be different. Analysis of these differences would require additional theoretical study.

Assuming that He^+ excitation is the same as H^+ excitation at these velocities, it is demonstrated in Figs. 3 and 7 that the theoretical calculations are qualitatively correct, but quantitatively in error. For instance, in Fig. 3 the theoretical curve has values of $\tilde{q}$ that are significantly smaller than those that were experimentally determined. The same is true for the $\tilde{q}$ values of the ^1S peak shown in Fig. 7. This curve, in addition, predicts that the asymptote is at a larger angle than experiments have indicated. This last discrepancy has been noted before.[6]

Figure 4 displays the $\tilde{q}'$ values for 700-keV Li^+ excitation and compares it to the theory of 100-keV H^+ excitation. The agreement is generally good except at backward angles, where theoretical predictions are larger than experiment. In this case, however, there is little reason to claim that the Li^+ excitation is similar to H^+ excitation. For instance, for 700-keV Li^+ there is considerable spin exchange in the excitation, as evidenced by the large $(2p^2)^3P$ peak that is seen in the emission spectrum (see Fig. 1). In the H^+ case, however, that excitation process is impossible.

B. The symmetric Shore parameter, $B'(\theta)$

Figures 9, 10, and 11 show the $B'(\theta)$ values for the three peaks studied with 500-keV/amu ions used as the projectiles. It should be stressed that in almost no case can the values of the electron emission intensity, as interpreted by $B'(\theta)$, be considered symmetric about the 90° emission angle. If no interferences were present, these curves would be symmetric. The ^1S peak, in addition, would necessarily be isotropic. When interferences with the continuum are present, however, this symmetry no longer exists.

The behavior of the ^1P peak (Fig. 9) is moderately charge dependent. He^+- and Li^+-induced peaks are roughly constant in size at angles greater than 90°, but at

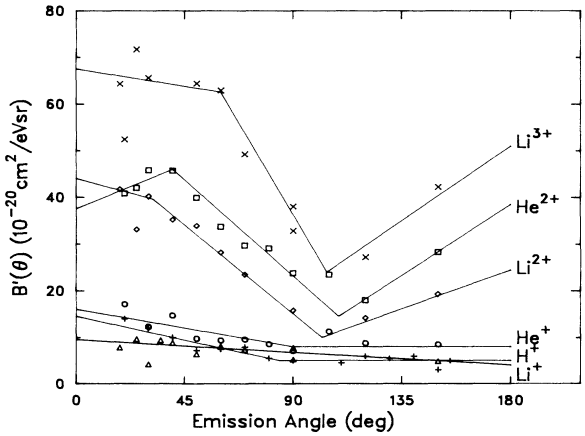

FIG. 9. The limit symmetric Shore parameter, $B'(\theta)$, of the $(2s2p)^1P$ peak. ○, 2000-keV $^4He^+$; △, 3500-keV $^7Li^+$; □, 2000-keV $^4He^{2+}$; ◇, 3500 keV $^7Li^{2+}$; ×, 3500-keV $^7Li^{3+}$; +, 500-keV H^+. The 500-keV H^+ data were obtained from Ridder (Ref. 7) and do not include the FIPCI. The lines are to guide the eye and as measures of total excitation yield.

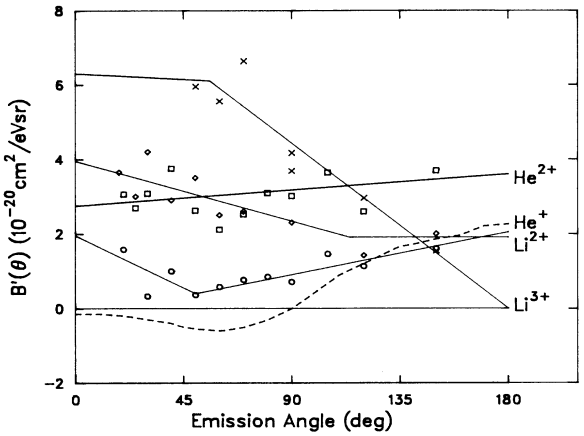

FIG. 10. The limit symmetric Shore parameter for the $(2s^2)^1S$ peak. The symbols represent the same ions as in Fig. 9. The dashed line is the theoretical predictions of this parameter for excitation by 500-keV H^+ (from Ref. 6).

forward angles they tend to get larger, increasing by a factor of about 2. As can be seen in Fig. 3(b), theory underestimates the magnitude of $B'(\theta)$ at forward angles.

Because of the large background, and because of the presence of the ^3P peak, the ^1S peak was not measurable for 3.5-MeV Li^+ projectiles. It was also not measurable at angles less than 50° for the 3500-keV Li^{3+} projectile. Nevertheless, fairly reproducible results for the other projectiles were obtained (Fig. 10). The He^+ induced peaks are largest at both forward and backward angles, with a minimum at about 50°. At no angle, however, does $B'(\theta)$ become negative (that is, the peak never becomes a window), either in the FIPCI model or in the actual peak. As can be seen in Fig. 10, theory predicts negative values at angles less than 90°.

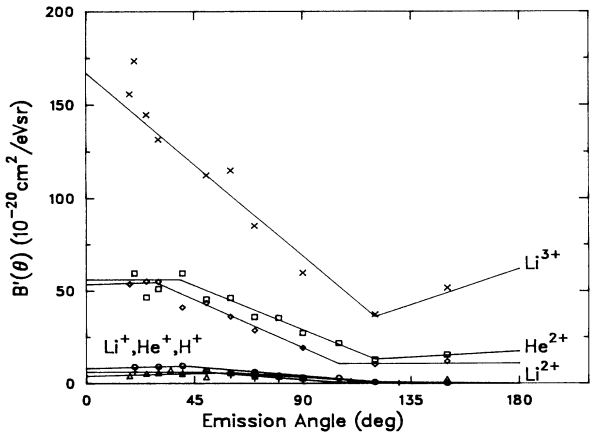

FIG. 11. The limit symmetric Shore parameters of the $(2p^2)^1D$ peak. The symbols represent the same ions as in Fig. 9.

The first observation to make about the ^1D peak (Fig. 11) is that the excitation of this peak is very charge dependent, with larger charges creating significantly larger peaks. Secondly, all the curves are roughly similar in shape, being smaller at backward angles and rising somewhat linearly to forward angles. In the case of singly charged ions the ^1D peak is very small at backward angles—at 150° it is a small bump on the side on the relatively large ^1P peak. At forward angles it is at least as large as the ^1P peak. For the other charged projectiles the same is true, but to a lesser degree.

C. Energy differences

Of the four peaks measured, the ^1P and ^1D peaks were fixed by the fitting program to be 0.237 eV apart. Thus, the fitted energy of the ^1D resonance was tied to the position of the ^1P resonance. The position of the ^1D state can then have a systematic error on the order of the error in the value of the energy separation. This error is estimated to be about 7 meV.[20] The other two resonances, i.e., the ^1S and the ^3P states, were often weak and sometimes could not be measured. In particular the ^3P peak could only be measured at backward angles and only for the 700-keV Li^+ projectile.

The ^3P to ^1D energy difference is 1.57±0.01 eV; the error is determined by the scatter of the ΔE values. For comparison, the best published data[20,33,34] indicate that the ^3P-^1D difference is 1.63±0.06 eV. There is much more data available for the determination of the ^1D to ^1S energy difference. This energy difference is 2.059±0.01 eV. The error is again the calculated standard deviation of the ΔE values. The averages and errors of the ΔE's, for each of the projectiles considered, were very consistent with each other. An evaluation of the published energy values for these two states reveals an energy difference of 2.08±0.04 eV. This average includes experimental and theoretical values.

Agreement above is good. The precision of the two energy-difference values reported here is better than any previously reported experiment and better than the range of values published in the literature.

VI. CHARGE DEPENDENCE OF THE SYMMETRIC SHORE PARAMETER

We can examine in more detail the charge dependence of the emission from these doubly excited states in order to study the excitation mechanism. The highly correlated first Born process may show a Q^2 dependence, while the uncorrelated second Born process could show a Q^4 dependence. An expected example of the latter may be in the excitation of the ^1D state. It is estimated that excitation of this state by electrons of energies less than about 3 keV is dominated by the path through the singly excited $(1s2p)^1P$ state.[33] This process is described by the second Born approximation. Intermediate charge dependences may be observed if two excitation mechanisms are comparable or if there is significant interference between them.

The use of the data shown in Figs. 9–11 for this purpose is questionable because the parameter $B'(\theta)$ is in

many cases dominated by interference, and is thus not a measure of excitation yield. This can easily be seen in Eq. (3.9) which is the limit formula for this parameter. That the parameter $B'(\theta)$ is not the yield is also demonstrated by its asymmetry about the 90° emission angle. As already discussed, the true emission by an isolated atom, when no coherent continuum is present, must decay symmetrically.

It is also not sufficient to integrate $B'(\theta)$ over all emission angle with the claim that interference only redistributes total intensity and does not destroy or create it. While this is true, the redistribution occurs primarily in energy, and not in emission angle. This effect is not completely treated by the theoretical approach leading to the derivation of the Shore parameters; this is clearly stated by Fano and Cooper in Ref. 26, where they discuss optical absorption by autoionizing Rydberg series. They say that one may consider the first-order discrete state as repelling the adjacent continuum states, much as close-lying atomic states can repel each other. If the repulsion is much greater than the intrinsic strength of the state, a window in the spectra will appear. This decrease in continuum intensity should be compensated by a weaker but widespread increase at different energies. The increase of the far wing intensity, however, is not described by the Beutler-Fano profile.[26] The previous comment may explain why the parameter $|b|^2$, which has the appearance of an emission yield, is also not symmetric about 90°.

As is evident in Figs. 9–11, the analysis of yield is further complicated by data that is both not smooth and has significant gaps across the angular range. This last complication is particularly true of the ^1S excitation by Li^{3+}, where $B'(\theta)$ must be guessed for angles less than 40°. There is also no general formula for the angular dependence of this parameter, and generic equations that may be used to fit the data (such as a sum of cosine terms), often lead to very anomalous results. We thus felt it simpler and more justified to draw several straight lines through the data and use these to determine the effective yield. These lines are the ones shown in Figs. 9–11. This method is strongly affected by judgment and the results should be considered with reasonable suspicion.

With the above reservations in mind, the effective total yield σ'_T is obtained by integrating Eq. (3.1) over energy and angle,

$$\sigma'_T = \sum_k \pi^2 \Gamma \int_{\theta_i}^{\theta_f} B'_k(\theta) \sin\theta \, d\theta \ , \tag{6.1}$$

where $B'(\theta)$ is one of the straight lines in Figs. 9–11 (labeled by k) and θ_i (θ_f) are the lower limit (upper limit) of that line. The results are shown in Table I. The values of σ'_T can be fit by the following function of projectile charge Q:

$$\sigma'_T(Q) = AQ^B \ , \tag{6.2}$$

where A and B are parameters.

The parameter B of the above equation is 1.16 for the ^1S peak, 1.55 for the ^1P peak, and 2.58 for the ^1D peak. Despite the obvious uncertainties we draw two conclusions: First, the charge dependences of the electron emissions from the ^1P and ^1S states is significantly less than the Q^2 dependence that is the expected minimum. Second, the ^1D excitation seems different in character than the excitation of the other two peaks, being much more charge dependent. This last observation might have been expected for reasons already alluded to—excitation of the ^1D state should be dominated by the second Born process, while excitation of the ^1S and ^1P states should not be.[35] Further explication will require a more detailed analysis of interference effects and excitation processes.

TABLE I. The total integrated emission cross section, in units of 10^{-20} cm^2, of the three peaks studied after excitation by some 500-keV/amu ions. The cross sections have an estimated precision of ±35%. Note: These values were obtained by integrating the straight lines shown in Figs. 10–12, and thus take account of the FIPCI. See text for a discussion of the difficulties in interpretation of these numbers. The H^+ cross sections were obtained from data measured by Ridder (Ref. 7).

	^1S	^1P	^1D
3500-keV $^7Li^{3+}$	11.8	34.4	110.5
2000-keV $^4He^{2+}$	8.8	22.2	45.1
3500-keV $^7Li^{2+}$	6.8	16.5	35.4
2000-keV $^4He^+$	2.9	7.3	6.2
3500-keV $^7Li^+$		5.0	3.8
500-keV H^+		5.2	4.4

VII. SUMMARY

To summarize, we examined the electron emission from doubly excited helium atoms. The atoms were excited by charged ions of 500-keV/amu or 100-keV/amu energy, and we determined cross sections that were differential in both electron energy and emission angle respective to the ion beam.

We demonstrated that, when peak profiles are measured, a post-collision interaction is important at surprisingly large projectile velocities. In fact, we estimate that this FIPCI should be included for a particular ion and emission angle when the value of C/V [see Eq. (3.4)] is greater than about 0.01. This means that (at least for these states) emission profiles at 0° may be affected by singly charged particles that have velocities of up to 13.5 a.u. (e.g., 4.5-MeV protons). We have demonstrated that most of the profile variation that has been observed (and unexplained) in ion excitation is caused by fast-ion PCI. This includes variation caused by different ion energies and by different observation angles, and is particularly true at forward emission angles.

For singly charged projectiles we found moderately good agreement with some theoretical predictions. This agreement, however, was only possible when the FIPCI is included in the analysis. There are still some significant discrepancies, however. For instance, the size of the $(2s2p)^1P$ peak is underestimated at forward angles, and the window nature of the $(2s^2)^1S$ peak at forward

angles is not reproduced by experiment. We find that these aspects of the profiles are intrinsic to the excitation process, and need to be accounted for in theory.

We found quite varied behavior of the limit peak profiles. The ^1S state, for instance, shows a systematic decrease in the angular position of the $\bar{q}'$ asymptote as the projectile charge increases. The ^1P peak, which has no asymptote of $\bar{q}'$, shows a tendency toward more symmetry as the ion charge increases. The ^1D peak, which has a backward-angle asymptote for singly charged ions, has none for doubly and triply charged ions.

Some states, such as the ^1D state, can have their emission peak profiles and intensities reliably categorized by the charge of the ion used to excite them. Other states, such as the ^1S state, cannot be so categorized. Thus, not surprisingly, the influence of the electrons carried with the projectile depends on which state is being excited.

In an analysis of emission intensity, we find that the ^1S and ^1P states show a less than "projectile-charged-squared" dependence for 500-keV/amu ions. The ^1D state, however, shows a significantly stronger dependence.

ACKNOWLEDGMENTS

One of us (P.W.A.) would like to thank Dr. Gordon Berry, Dr. Alan Gallagher, and Dr. Ugo Fano for helpful discussions and support. Dr. R. Bruch, Dr. D. Zei, and W. Stoffler provided valuable experimental help. This research was performed at Argonne National Laboratory under the auspices of the U.S. Department of Energy (Office of Basic Energy Sciences) under Contract No. W-31-109-Eng-38.

*Present address: Joint Institute for Laboratory Astrophysics, University of Colorado and National Bureau of Standards, Boulder, CO 80309-0440.

[1]P. W. Arcuni, Phys. Rev. A **33**, 105 (1986).
[2]U. Fano, Phys. Rev. **124**, 1866 (1961).
[3]V. V. Balashov, S. S. Lipovetsky, and V. S. Senashenko, Zh. Eksp. Teor. Fiz. **63**, 1622 (1972) [Sov. Phys.—JETP **36**, 858 (1973)].
[4]V. V. Balashov, S. S. Lipovetsky, and V. S. Senashenko, Phys. Lett. **40A**, 389 (1972).
[5]S. S. Lipovetsky and V. S. Senashenko, J. Phys. B **5**, L183 (1972).
[6]S. S. Lipovetsky and V. S. Senashenko, J. Phys. B **7**, 693 (1974).
[7]D. Ridder, diplomarbeit, Freie Universitat Berlin, 1973 (unpublished).
[8]M. Prost, diplomarbeit, Freie Universitat Berlin, 1978 (unpublished).
[9]M. E. Rudd, Phys. Rev. Lett. **13**, 503 (1964).
[10]F. D. Schowengerdt and M. E. Rudd, Phys. Rev. Lett. **28**, 127 (1972).
[11]N. Stolterfoht, Phys. Lett. **37A**, 177 (1971).
[12]N. Stolterfoht, D. Ridder, and P. Ziem, Phys. Lett. **42A**, 240 (1972).
[13]A. Bordenave-Montesquieu, A. Gleizes, M. Rodiere, and P. Benoit-Cattin, J. Phys. B **6**, 1997 (1973).
[14]A. Bordenave-Montesquieu, P. Benoit-Cattin, M. Rodiere, A. Gleizes, and H. Merchez, J. Phys. B **8**, 874 (1975).
[15]A. Bordenave-Montesquieu, A. Gleizes, and P. Benoit-Cattin, Phys. Rev. A **25**, 245 (1982).
[16]A. Bordenave-Montesquieu, P. Benoit-Cattin, A. Gleizes, and H. Merchez, J. Phys. B **8**, L350 (1975).
[17]K. D. Sevier, *Low Energy Electron Spectrometry* (Wiley, New York, 1972).
[18]N. Stolterfoht, Hahn-Meitner-Institute Berlin, Bericht 104, 1971 (unpublished).
[19]M. E. Rudd, L. H. Toburen, and N. Stolterfoht, At. Data Nucl. Data Tables **18**, 413 (1976).
[20]W. Shearer-Izumi, At. Data Nucl. Data Tables **20**, 531 (1977).
[21]N. H. Draper and H. Smith, *Applied Regression Analysis* (Wiley, New York, 1966).
[22]David L. Ederer, Appl. Opt. **8**, 2315 (1969).
[23]P. W. Arcuni, Ph.D. thesis, University of Chicago, 1985 (unpublished).
[24]B. W. Shore, Rev. Mod. Phys. **39**, 439 (1967).
[25]B. W. Shore, J. Opt. Soc. Am. **57**, 881 (1967).
[26]U. Fano and J. W. Cooper, Phys. Rev. A **137**, 1364 (1965).
[27]R. B. Barker and H. W. Berry, Phys. Rev. **151**, 14 (1966).
[28]P. van der Straten and R. Morgenstern, J. Phys. B **19**, 1361 (1986).
[29]M. Yu. Kuchiev and S. A. Sheinerman, Zh. Eksp. Teor. Fiz. **90**, 1680 (1986) [Sov. Phys.—JETP **63**, 986 (1986)].
[30]P. van der Straten and R. Morgenstern, Phys. Rev. A **34**, 4482 (1986).
[31]A. Z. Devdariani, V. W. Ostrovskii, and Yu. N. Sebyakin, Zh. Eksp. Teor. Fiz. **73**, 412 (1977) [Sov. Phys.—JETP **46**, 215 (1977)].
[32]V. N. Mileev, V. S. Senashenko, and E. Yu. Tsymbal, J. Phys. B **14**, 2625 (1981).
[33]W. C. Martin, J. Phys. Chem. Ref. Dat. **2**, 257 (1972).
[34]P. J. Hicks and J. Comer, J. Phys. B **8**, 1966 (1975).
[35]S. S. Lipovetsky and V. S. Senashenko, Opt. Spektrosk. **34**, 1046 (1973) [Opt. Spectrosc. (USSR) **34**, 607 (1973)].